■ **Ionic Liquids**

Highly Luminescent and Color-Tunable Salicylate Ionic Liquids

Paul S. Campbell,[a] Mei Yang,[a] Demian Pitz,[a] Joanna Cybinska,[a, b] and Anja-Verena Mudring*[a, c]

In memory of John D. Corbett

Abstract: High quantum yields of up to 40.5% can be achieved in salicylate-bearing ionic liquids. A range of these ionic liquids have been synthesized and their photoluminescent properties studied in detail. The differences noted can be related back to the structure of the ionic liquid cation and possible interionic interactions. It is found that shifts of emission, particularly in the pyridinium-based ionic liquids, can be related to cation–anion pairing interactions. Facile and controlled emission color mixing is demonstrated through combining different ILs, with emission colors ranging from blue to yellow.

Introduction

With decreasing availability and increasing cost of lanthanides, alternative luminescent materials are highly sought after. In comparison, luminescent organic materials are economically very attractive; they can be synthesized from readily available materials, and in contrast to most lanthanides, their electronic transitions may be formally allowed, thus strong absorption and high emission intensities can be easily envisaged. For example, organic light-emitting diodes OLEDs currently represent a rapidly growing area of interest based on electroluminescent organic molecules,[1–8] with many new energy efficient and flexible displays being based on this innovative technology. Furthermore, organic dyes are currently used in dye-lasers,[9] and may be applied as sensitizers to enhance lanthanide luminescence.[10–12] One great set-back with organic fluorophores is their photodegradation, meaning that after a certain time, the dyes must be replaced.[13] However, it has already been reported that incorporating such dyes into ionic liquids can enhance their photostability.[14, 15]

The field of ionic liquids (ILs) has experienced an explosion in research during the last two decades.[16–18] This can be attributed in part to their unique and interesting physicochemical properties such as low volatility, large liquids range, wide electrochemical window, nanostructuration, and so on. Furthermore, ILs are inherently adaptable media, with countless different anion–cation combinations available and facile modifications possible. They are therefore described as "designer solvents", and can indeed be tailored to specific tasks. As such, they have been used in diverse fields from catalysis[16, 19–24] and separations[25–27] to electrochemistry[28, 29] and nanosynthesis.[30–39] An ever-increasing number of fields are witnessing the introduction of ionic liquids.[40] For example, ionic liquids have recently been used in the production of new luminescent materials. Introduction of transition metal or lanthanide ions is seen to lead to highly luminescent imidazolium-based ILs,[41–46] whereas the aptitude of ILs as media for nanochemistry has enabled their application in the synthesis of lanthanide-based nanophosphors.[47–54] Following on from this, our group has recently reported the one-pot synthesis of luminescent polymer–nanoparticle composites, based on a polymerizable IL.[55]

ILs are often based on aromatic moieties such as imidazolium or pyridinium, and therefore exhibit intrinsic luminescence thanks to low-lying π–π* transitions, as has been previously studied and reported.[56–58] Unfortunately, the luminescence of these common ILs is weak, inefficient and unexploitable. However, thanks to their aforementioned adaptability, ionic liquids specifically designed to exhibit strong luminescence have recently been brought into the fold. For example, Deng and co-workers has reported turquoise-emitting quinolizinium salts,[59] as well as functionalized imidazolium moieties,[60] whereas Boydston et al. described property-tunable fluorophores based on a benzobisimidazolium-fused ring system, displaying high quantum yields in solution.[61, 62] Furthermore, a paper by Huang et al. describes a strongly photoluminescent ionic liquid based on a large cationic dendrimer.[63] Herein, we report the facile synthesis and optical characterization of highly luminescent ionic liquids based on the salicylate anion, varying the

[a] Dr. P. S. Campbell, M. Yang, D. Pitz, Dr. J. Cybinska, Prof. A.-V. Mudring
Anorganische Chemie III, Materials Engineering and Characterisation
Fakultät für Chemie und Biochemie, Ruhr-Universität Bochum
Universitätsstrasse 150, 44801 Bochum (Germany)
Fax: (+49) 2343214951
E-mail: anja.mudring@rub.de

[b] Dr. J. Cybinska
Faculty of Chemistry, Faculty of Chemistry
University of Wrocław, Joliot-Curie 14, 50383 Wrocław (Poland)

[c] Prof. A.-V. Mudring
Materials Science & Engineering, Iowa State University
and Critical Materials Institute, Ames Laboratory, Ames, IA 50011 (USA)
E-mail: mudring@iastate.edu

⬛ Supporting information for this article is available on the WWW under
http://dx.doi.org/10.1002/chem.201301363.

employed cation to control the resultant luminescent properties.

Results and Discussion

In this study, a series of ionic liquids was synthesized bearing the salicylate anion through a standard anion methathesis reaction by using sodium salicylate and the corresponding cation halides. The salicylate (2-hydroxybenzoate) anion, [Sal], consists of a benzene ring bearing *ortho* hydroxyl and carboxylate groups as shown in Scheme 1. Commonly used ionic liquid cations were chosen, and could be divided into three
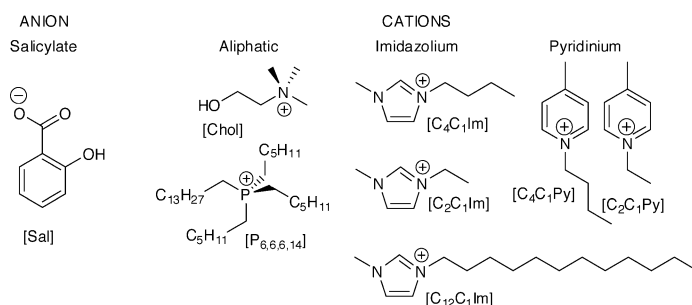
Scheme 1. Structure and abbreviations of the anion and cations used in this study.

groups based on their structures as shown in Scheme 1: 1) Aliphatic: choline [Chol], trihexyltetradecylphosphonium [$P_{6,6,6,14}$]; 2) Imidazolium: 1-ethyl-3-methylimidazolium [C_2C_1Im], 1-butyl-3-methylimidazolium [C_4C_1Im], and 1-dodecyl-3-methylimidazolium [$C_{12}C_1Im$]; and 3) Pyridinium: 1-ethyl-4-methylpyridinium [C_2C_1Py], 1-butyl-4-methylpyridinium [C_4C_1Py]. Thus, it was possible to gauge the effect of varying degrees of aromaticity in the cation on the subsequent properties as well as the effect of the length of alkyl substituents (e.g., ethyl vs. butyl). [Chol][Sal], [$P_{6,6,6,14}$][Sal], [C_2C_1Im][Sal] and [C_4C_1Im][Sal] were isolated as free-flowing pale-yellow-tinted clear liquids. [$C_{12}C_1Im$][Sal] was obtained as a white solid. [C_2C_1Py][Sal] and [C_4C_1Py][Sal] were isolated as orange/brown viscous and free-flowing liquids, respectively.

Impurities in the ionic liquids under study cannot be ignored as they may also play a decisive role in the luminescent properties; for example, they may be photoactive, or manifest a quenching effect. The purities were therefore thoroughly assessed through elemental analysis, Karl Fischer coulometry and both positive and negative ion chromatography to assess halide and sodium levels. Elemental analyses matched well with expected values, and Karl Fischer measurements showed that although water content in the crude products lay around 2 wt.%, this could be considerably reduced (<600 ppm) by simply drying for three days under a dynamic vacuum at 50 °C. Inorganic salt levels could be reduced by precipitation in dichloromethane and filtration over Celite. The resultant halide content (bromide or chloride, depending on the starting salt) was found to range from 0.080 ([C_2C_1Py]) to 1.3 wt.% ([C_2C_1Im]), whereas in each case the sodium content was found to be very low (0.062 for [C_2C_1Py] to 0.60 wt.% for

[Chol]). All measured values can be found in the Experimental Section.

Thermal and structural characterization

Representative differential scanning calorimetry (DSC) thermograms of the as-synthesized ionic liquids are depicted in Figure 1, with important phase transitions for all ILs tabulated in Table 1. All other thermograms can be found Figure S1 in the Supporting Information. It can be seen that all investigated compounds could be classed as ionic liquids, with a liquid phase observed below 100 °C. With the exception of [$C_{12}C_1Im$], all cations gave room-temperature ionic liquids, presenting low glass transition temperatures (T_g) in the DSC thermograms. During the DSC measurement, the IL [Chol][Sal] also underwent a cool crystallization immediately prior to melting, indicated by the appearance of consecutive broad *exo*- and endothermic transitions at 8.2 and 37.7 °C, during the second and subsequent heating cycles. This crystallization was confirmed by using polarized optical microscopy (POM) analysis, in which crystal growth was observed at 8 °C upon heating. In all cases the butyl-bearing ILs presented lower T_g values than their ethyl-bearing counterparts. This is a common result in ILs, because

Table 1. Important phase transitions of salicylate ionic liquids.

Entry	Cation	T_g (heating) [°C] (ΔC_p [J g^{-1} K^{-1}])	T_g (cooling) [°C] (ΔC_p [J g^{-1} K^{-1}])	T_m (heating) [°C] (ΔH [J g^{-1}])
1	[Chol][a]	−54.0 (1.39)	−47.0 (1.12)	37.7 (93.2)
2	[$P_{6,6,6,14}$]	−79.6 (1.05)	−67.4 (1.00)	–
3	[C_2C_1Im]	−47.7 (0.80)	−39.8 (0.72)	–
4	[C_4C_1Im]	−54.1 (0.84)	−49.9 (0.75)	–
5	[$C_{12}C_1Im$][b]	–	–	48.0 (116.7)
6	[C_2C_1Py]	−39.6 (0.66)	−27.9 (0.63)	–
7	[C_4C_1Py]	−67.7 (1.13)	−60.5 (0.73)	–

[a] Cold crystallization on heating onset 8.2 °C (−97.6 J g^{-1}). [b] Supercooled SmC liquid crystal 50–19.5 °C.

the effect of increasing the entropic barrier to crystallization by increasing the length of the alkyl chain tends to outweigh the effect of increasing molecular weight until an intermediate chain length around 8, after which the temperature of melting transitions starts to increase, owing to increasing van der Waals interactions between the long alkyl chains.[17]

As could be expected, [$C_{12}C_1Im$] exhibited the most complex thermal behavior (thermograms for the second cooling and heating runs are given in Figure 2 a.) Upon heating, a broad exothermic peak with onset at 48 °C indicates a transition from the solid-to-liquid state. However, upon cooling over the same range, two distinctly separate phase transition events were observed. Firstly, a small exothermic peak with onset at 50 °C is noted. This is followed by a large exothermic peak with onset at 19 °C, presenting several local maxima. The latter can be assigned as crystallization, with the several maxima due to the possibility of several solid–solid phase transitions. The phase
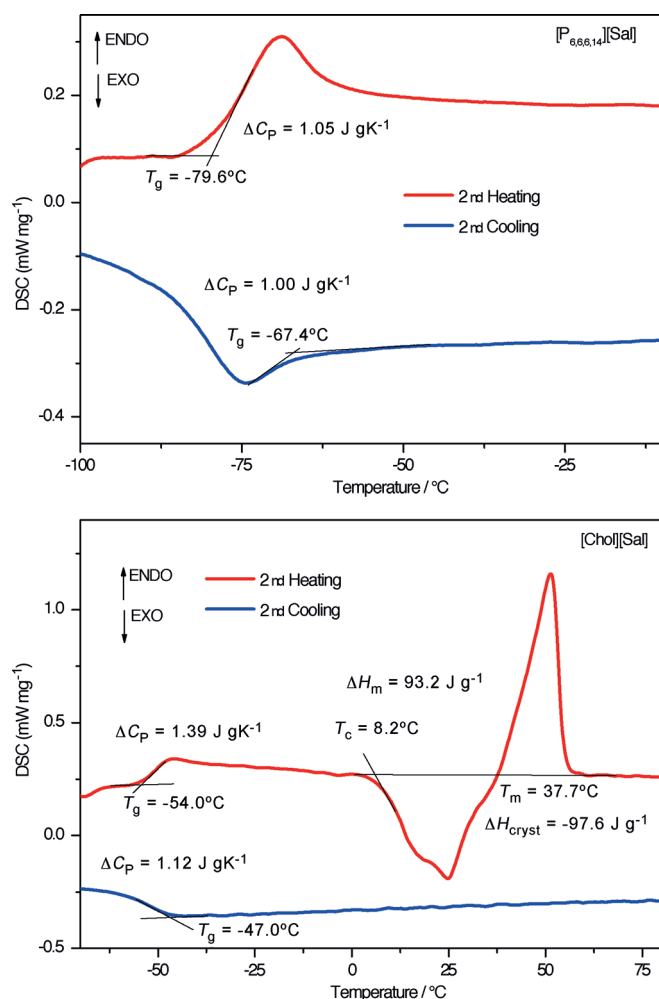
Figure 1. Example DSC thermograms of as-synthesized ionic liquids (top [P$_{6,6,6,14}$][Sal], center [Chol][Sal]) measured at heating/cooling rate of 10 K min^{-1}. Only second cycles are shown; subsequent cycles were identical in each case. Bottom: Polarizing optical micrograph of [Chol][Sal] crystals grown at 8 °C on heating from −40 °C at 10 K min^{-1}.

present from 50–19 °C may be assigned to a supercooled liquid-crystalline phase. Indeed, the [C$_{12}$C$_1$Im] cation has already been well-studied and has been found to be prone to

the formation of mesophases.[64,65] POM and small-angle X-ray scattering (SAXS) measurements, indeed confirm the occurrence of a supercooled ionic liquid crystal (Figure 2 b–d). The oily streak texture observed in the POM image taken at 29 °C upon cooling is typical of a smectic phase. Multiple reflections are visible in the X-ray scattering patterns at 30 °C upon heating recorded on the small- and wide-angle range, due to the different lattice planes in the crystalline material. Upon cooling, only one reflection can be observed in the small-angle range, corresponding to an interlayer distance in the mesophase of 27.65 Å, whereas only a broad reflection of amorphous character is observed in the wide-angle range (note that the apparent doubling of peaks is due to the SAXS experimental set-up.). According to the SAXS data, at the same temperature in the crystal phase, the interlayer distance is larger at 28.54 Å. This observation could be explained by the formation of a smectic C mesophase, in which the interlayer distance shortens in the liquid crystal (LC) phase due to a tilt of the alkyl chains away from the normal of the layer plane, as illustrated in Scheme 2.
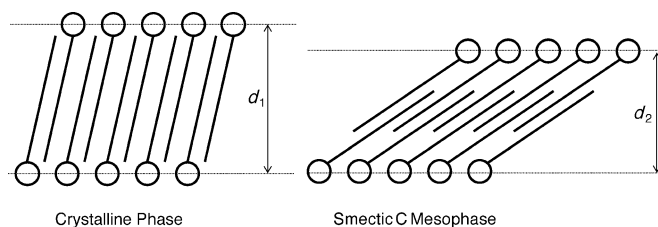
Scheme 2. Illustration of different d-spacings in the crystalline phase and the smectic C mesophase.

Structural and environmental properties are well-known to play an important role in the resultant luminescence of organic molecules.[66] Intermolecular interactions have also been reported to strongly influence luminescent properties. For example, the fluorescence of cyanine molecules has previously been shown to be highly dependent on the intermolecular arrangement, with π-stacking leading to blue- or redshifted emission depending on the orientation.[67] Furthermore, certain molecules are known to form excited dimers (excimers) when excited, which have a redshifted emission compared with the monomer itself. Such behavior is commonly observed in fused polyaromatics such as naphthalene or pyrene.[68] Another possibility is non-radiative excitation energy-transfer between neighboring molecules. This requires Coulombic interactions and/or intermolecular orbital overlap as well as short distances between molecules.[66] Herein, the effect of intermolecular/interionic interactions will be observed, because although the emitting moiety in this study, the salicylate anion, is not changed, its chemical environment varies with each different cation used. The effects on photoluminescence will be discussed later in detail.

One inherent property of ionic liquids is their high entropic barrier to crystallization. Indeed, for this reason, crystals of sufficient quality for X-ray analysis could not be obtained for the synthesized compounds. Despite this, molecular dynamics sim-
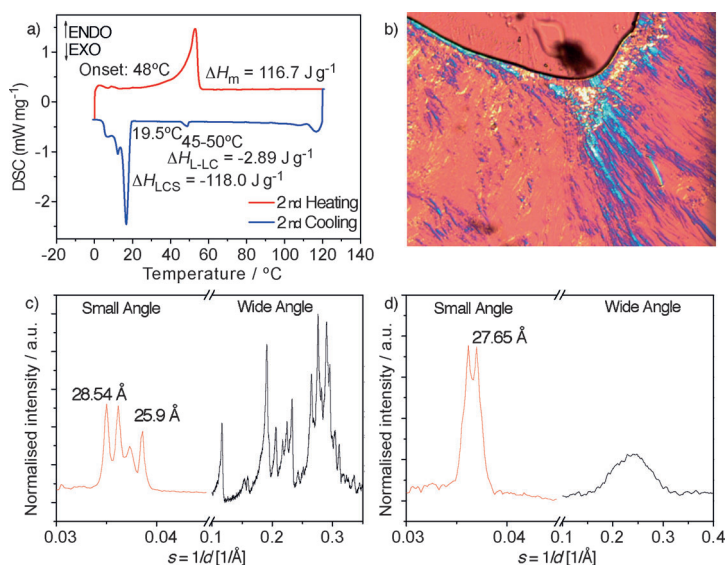
Figure 2. a) DSC thermogram of $[C_{12}C_1Im][Sal]$ recorded with a heating/cooling rate 10 K min^{-1}; b) Polarizing optical micrograph of $[C_{12}C_1Im][Sal]$ taken at 29 °C upon cooling at 10 K min^{-1}. X-ray scattering patterns in both small- and wide-angle range of $[C_{12}C_1Im]$-[Sal] recorded at c) 30 °C upon heating, and d) 30 °C upon cooling.

ulations, coarse-grain modelling and X-ray analysis have previously shown that a significant structuration exists on the nanoscale even in the purely liquid state of ionic liquids.[69–71] Therein, non-polar alkyl chains would group together in micellar-type aggregates, segregated by ionic channels resulting from the anion and cation head-group. 2D NMR spectroscopic techniques could be employed utilizing the nuclear Overhauser effect (NOE) to detect through-space interionic interactions. Such techniques have previously been used to determine interactions between IL solvents and organic substrates.[22] Specifically, rotating frame NOE spectroscopy (ROESY) is suitable for obtaining positive NOEs despite the long rotational correlation times possible. In ^{1}H-^{1}H ROESY techniques, correlations are established from through-space cross relaxation between nuclear spins during the mixing period. The selective irradiation of a proton group affects the intensities of integrals of all-proton groups that are spatially close (max 4–5 Å) but not necessarily connected by chemical bonds.[72] The ROE signal strength varies with the inverse sixth power of the corresponding interatomic distance, $I \propto 1/r^6$. In the liquid state, this relationship is possible if the intermolecular association is close enough to turn the intermolecular relaxation into "intramolecular" within the ion pair or ion–molecule association.[73] To obtain well-resolved spectra, solutions of the ILs were prepared by dissolving 5 mg in 0.5 mL $[D_6]DMSO$, which was used to lock the NMR probe. For most ILs measured in this way, only diagonal and intra-ionic cross-peaks were observed, due to the dissolution in $[D_6]DMSO$. However, in the case of both pyridinium-based ILs, interionic interactions could also be observed. The ^{1}H-^{1}H ROESY NMR spectra and atomic assignment of $[C_2C_1Py][Sal]$ and $[C_4C_1Py][Sal]$ are given in Figure 3. In spite of the dissolution, correlation between positions on the separate aromatic rings can be clearly detected (circled in Figure 3. This presents clear evidence of a close anion–cation association,

probably proceeding through a combination of Coulombic attraction and π-stacking interactions. Interestingly, a cross-peak is also observed correlating the protons at the terminal position of the ethyl group to the δ-position of the salicylate ion in the case of $[C_2C_1Py][Sal]$. Indeed, it has previously been reported that in the case of imidazolium ILs, the short length of the ethyl chain does not allow for the segregation of polar and non-polar domains,[69] which may account for the apparent proximity of the alkyl chain to the anion in this case. The fact that no interionic cross-peaks are observed in the spectra of the other ILs does not necessarily mean that cation–anion interactions do not exist. However, this result does suggest that a notably stronger association exists in the pyridinium-based ionic liquids. This may be due in part to the matching symmetry of anion and cation (6-membered aromatic rings), allowing effective orbital overlap.

Optical characterization

The ionic liquids produced were found to display varying colors depending on the cation. Whereas those based on aliphatic and imidazolium ions were isolated as clear liquids with a slight yellow tint, orange/brown colors were observed for pyridinium-based ILs. These colors correspond to neither the isolated cations nor anions (based on the observed colors of the respective sodium or halide salts), thus must be due to the association of ions. To investigate this, UV/Visible absorption spectra were first acquired for ethanolic solutions of each salt prepared and compared to that of the sodium salt. For clarity, example spectra are given in Figure 4, representative of each for the three groups of cations under study compared to the spectrum of sodium salicylate. Other spectra are highly similar to their respective group and are given in Figure S2 (the Supporting Information), alongside spectra of the cation halides in Figure S3 (the Supporting Information), for comparison. The UV/Visible spectrum of the sodium salicylate salt shows three main bands, centered at 203 ($\varepsilon = 17\,500$), 228 ($\varepsilon = 3400$), and 297 nm ($\varepsilon = 2100$ L mol^{-1} cm^{-1}), which can be attributed to $\pi \rightarrow \pi^*$ and $n \rightarrow \pi^*$ electronic transitions in the salicylate ion. When coupled with the aliphatic $[P_{6,6,6,14}]$ or [Chol] cations, the absorption spectra remain unchanged. However, when coupled with any of the imidazolium cations, increased absorption is noted from 200 to 230 nm, as a result of the imidazolium $\pi \rightarrow \pi^*$ transitions. More strikingly, the absorption of $[C_2C_1Py][Sal]$ is notably stronger from 215 nm upwards, with a clear additional band centered at 260 nm. Furthermore, in this case, a clear absorption tail is apparent far into the visible range of the spectrum, hence giving an orange/brown color to this ionic liquid. This absorption can be attributed to ion-pair aggregates held together through Coulombic attraction and π-stacking even in dilute solution, corroborated by the ROESY NMR spectroscopic results. No evidence of ion-pairing could be seen between the salicylate and imidazolium or aliphatic cations.
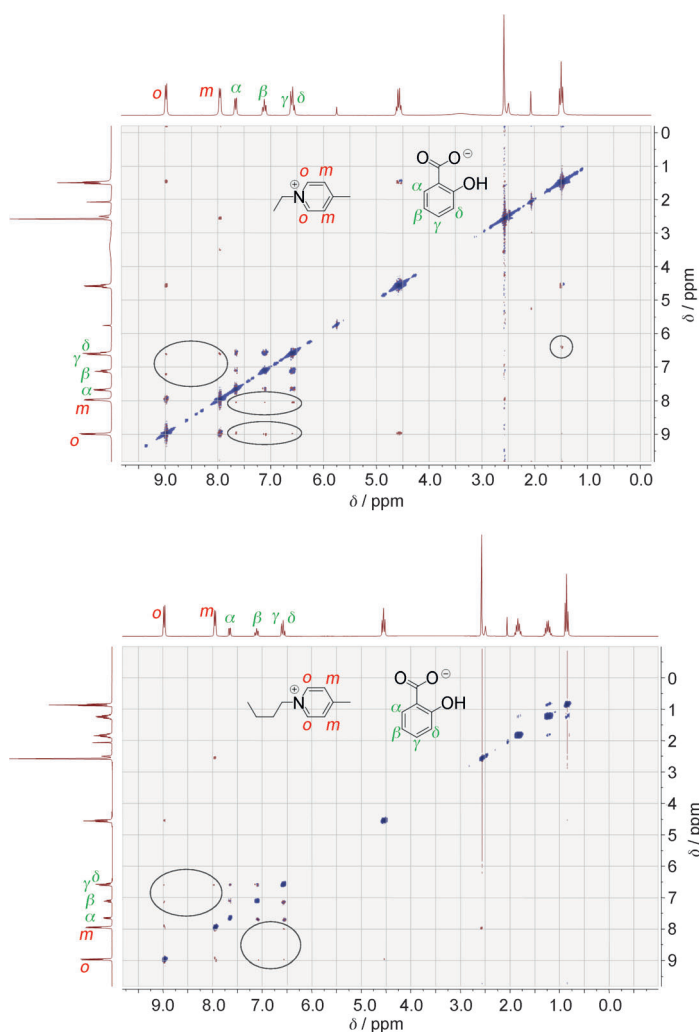
Figure 3. ^{1}H-^{1}H ROESY NMR spectrum of [C$_2$C$_1$Py][Sal] (top) and [C$_4$C$_1$Py][Sal] (bottom) recorded in [D$_6$]DMSO. For clarity, interionic correlation cross-peaks are circled.
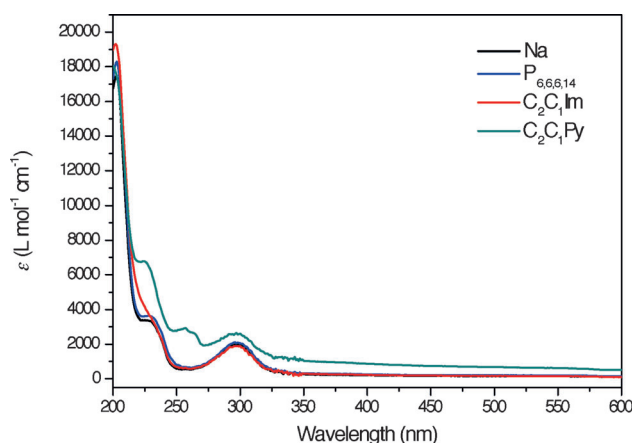

Figure 4. UV/Vis absorption spectra of the salicylate ILs in ethanol solution compared to that of the sodium salt.

Photoluminescence (PL) spectra of the pure ionic liquids were recorded at room temperature (25 °C) and compared to that of pure sodium salicylate. Normalized spectra are given in

Figure 5, with corresponding data summarized in Table 2. Excitation spectra are given in the Supporting Information. Emission maxima were taken as the maxima of Gaussian distribution functions fitted to the experimental data by using Origin software. Example emission spectra of one IL from each cation group are shown in Figure 5a. Despite the fact that the same species (salicylate anion) is responsible for emission in each case, stark differences can be seen in the resultant spectra. Firstly, a hypsochromic shift of emission was noted for the aliphatic cations compared with the sodium salt; the emission maxima were recorded at (399.4 ± 0.2) and (405.3 ± 0.2) nm for [P$_{6,6,6,14}$] and [Chol] (Figure 4b), respectively, whereas the sodium salt emission maximum appears at (422.5 ± 0.2) nm. This can be rationalized in terms of cation bulk. Compared with sodium, the ionic liquid cations [Chol], and especially [P$_{6,6,6,14}$], present a considerable bulk and therefore inhibit the close proximity between salicylate ions needed for the energy-lowering π–π interactions. Because [P$_{6,6,6,14}$] is considerably bulkier than [Chol], the effect for this cation is more pronounced.

Similarly, all ILs constituted of imidazolium cations also displayed a hypsochromic shift compared with the sodium salt, with emission maxima recorded at (405.1 ± 0.2), (404.3 ± 0.2), and (406.8 ± 0.4) nm for [C$_2$C$_1$Im], [C$_4$C$_1$Im], and [C$_{12}$C$_1$Im], respectively (Figure 4c). Such values can no longer be attributed solely to cation bulk, considering the fact that the largest of the group presents counterintuitively the longest wavelength emission. As previously stated, pure imidazolium ionic liquids present a certain structure, segregated into non-polar domains, comprising the aggregation of alkyl chains, and polar channels, in which anion and cation head-groups are found in close proximity. This would explain why regardless of the length of the alkyl chain, the distance between neighboring salicylate anions and thus maximum emission wavelength do not vary greatly. Furthermore, as the PL measurements were conducted at room temperature (25 °C), at which according to DSC and SAXS results [C$_{12}$C$_1$Im][Sal] exists as a crystalline solid, closer proximity between anions can be expected, pro-

Table 2. Photoluminescence data of salicylate ILs measured.

Entry	Cation	λ_{ex} [nm]	Maximum λ_{em} [nm]	Quantum yield (error) [%]
1	[Chol]	340	405.3 ± 0.2	40.5 (4.9)
2	[P$_{6,6,6,14}$]	340	399.4 ± 0.2	8.1 (0.9)
3	[C$_2$C$_1$Im]	340	405.1 ± 0.2	13.6 (0.2)
4	[C$_4$C$_1$Im]	340	404.3 ± 0.2	23.3 (2.90)
5	[C$_{12}$C$_1$Im] (S)[a]	340	406.8 ± 0.4	35.9 (3.8)
	[C$_{12}$C$_1$Im] (LC)[b]	340	403.1 ± 0.2	not determined
6	[C$_2$C$_1$Py]	420	599.2 ± 0.4	3.95 (0.43)
7	[C$_4$C$_1$Py]	420	573.2 ± 0.6	2.67 (0.39)

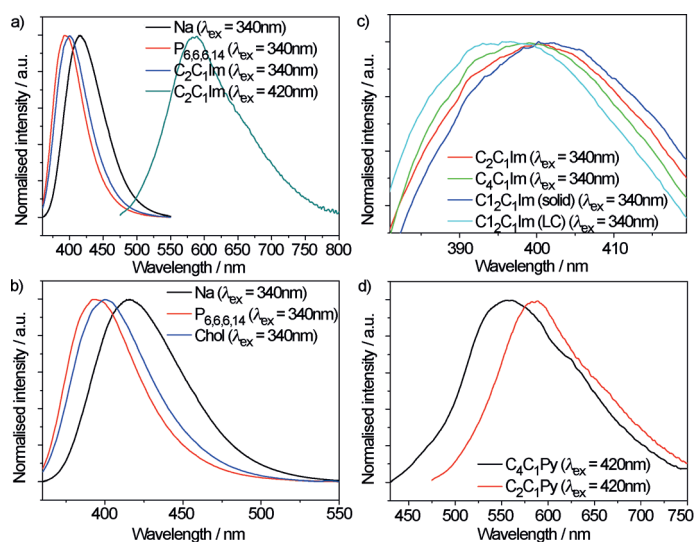[a] (S): Crystalline solid. [b] (LC): Liquid-crystal phase.

Figure 5. Comparison of the normalized emission spectra of salicylate ILs. λ_{ex}: excitation wavelength; (LC): denotes that the sample was measured in the liquid-crystalline state.

voking the longer wavelength emission observed. For comparison, the emission spectrum was also recorded for the supercooled liquid-crystalline compound at room temperature. In this state the emission maximum is shifted to (403.1 ± 0.2) nm, corresponding to increased disorder, as expected in the liquid-crystalline state compared with the perfectly ordered crystalline state. Again, no evidence for strong imidazolium-salicylate ion-pairs created through strong π–π and Coulombic interactions is observed. This is likely due to the mismatching symmetry (6-membered vs. 5-membered aromatic ring).

Interestingly, in the case of the pyridinium ionic liquids in this study, $[C_4C_1Py][Sal]$ and $[C_2C_1Py][Sal]$, both excitation and emission maxima experience large bathochromic shifts, effectively converting blue to yellow light. In Figure 4a, it can clearly be seen that the emission band of $[C_2C_1Py][Sal]$ displays a different vibrational structure to $[Na][Sal]$. This, along with the shifted excitation, provides a clear indication that the salicylate anion is not alone responsible for the observed fluorescence. Furthermore, changing the alkyl chain length has a significant effect on emission maximum, falling at (573.2 ± 0.6) and (599.2 ± 0.4) nm for $[C_4C_1Py]$ and $[C_2C_1Py]$, respectively (Figure 4d). This provides conclusive evidence for the involvement of the pyridinium moiety, however, ILs based on pyridinium coupled with optically inactive anions have been previously shown to present emission maxima in the blue region.[58] Because no "normal" salicylate or pyridinium fluorescence is detected, we can only attribute the observed photoluminescence behavior to the strong ion-pairs, previously evidenced by ROESY NMR spectroscopy. The strong ion-pair interactions would effectively create moieties exhibiting a more extensive π-system than in the individual ions. Increasing the number of π-electrons in a molecule is well-known to provoke an increase in absorption and emission wavelength, as can be seen in the oligacene or oligorylene series.[66] Shortening the alkyl chain reduces steric hindrance, and allows the ions to bind more strongly, and the emission is further redshifted.

Quantum yields of the ionic liquids were measured at 25 °C and results are given in Table 2. For most ILs, relatively high quantum yields were recorded, the highest being attributed to choline salicylate with (40 ± 5)%. It is highly interesting that these fluid systems, based on organic molecules whose high-energy vibrations could easily quench emission, display quantum yields of the same order of magnitude as the solid sodium salt. Pyridinium-based ionic liquids unfortunately suffer from relatively poor emission intensities and also as seen, poor quantum yields. This may be due to strong reabsorption of emitted light by these colored compounds, as well as the relative ease of quenching longer wavelength emission through vibrational relaxation. The varying efficiencies of the different ILs may also in part be related to the impurities. For example, the presence of bromide may increase the photoluminescence quenching through the external heavy atom effect, whereby relaxation through spin-orbit coupling increases with the fourth power of the atomic number.[66] This may explain the relatively low quantum yield of the $[C_2C_1Im]$ system in which the bromide precursor was employed, compared with the other imidazolium systems synthesized from the respective chloride salts, and in which a relatively high amount of bromide remained as an impurity. Furthermore, the small quantities of water may affect the efficiency, because water-induced fluorescence quenching has been reported, occurring through reorganization of hydrogen-bonding interactions in the excited state.[74] Molecular oxygen is also known to play a role in fluorescence quenching through excitation into low-lying singlet states.[66] For this reason the ILs were thoroughly dried and stored under inert atmosphere.

For lighting applications, white emitters are highly sought after. In modern white LEDs, white light is achieved through the combination of blue and yellow light; a blue-emitting semiconductor (e.g., InGaN) is coated with a blue-to-yellow light-converting phosphor material (e.g., $YAG:Ce^{3+}$). In our series of synthesized ILs, we observed both UV-blue and blue-yellow fluorescence. We could therefore transpose the aforementioned principle of white emission to our materials, by mixing a UV-blue fluorophore (e.g., $[Chol][Sal]$) with a yellow-blue fluorophore (e.g., $[C_4C_1Py][Sal]$), and measuring the emission of the resultant mixtures. Normalized emission spectra for different mixtures are given in Figure 6 (left), in which x denotes the molar fraction of $[C_4C_1Py][Sal]$. From these spectra it was possible to calculate the color coordinates of each mixture in the standard Commission Internationale de l'Eclairage (CIE) color space,[75] as shown in Figure 6 (center). Photographs of the mixed ILs in quartz tubes under 366 nm excitation are also given in Figure 6 (right). It can clearly be seen that by this method, color mixing was successful by a simple mixture of the ILs. The color coordinates are found on a pseudo-straight line between the deep-blue emission of pure $[Chol][Sal]$ $(x=0)$ and the yellow emission of pure $[C_4C_1Py][Sal]$ $(x=1)$. Amongst the samples studied, it can be seen that the sample giving the
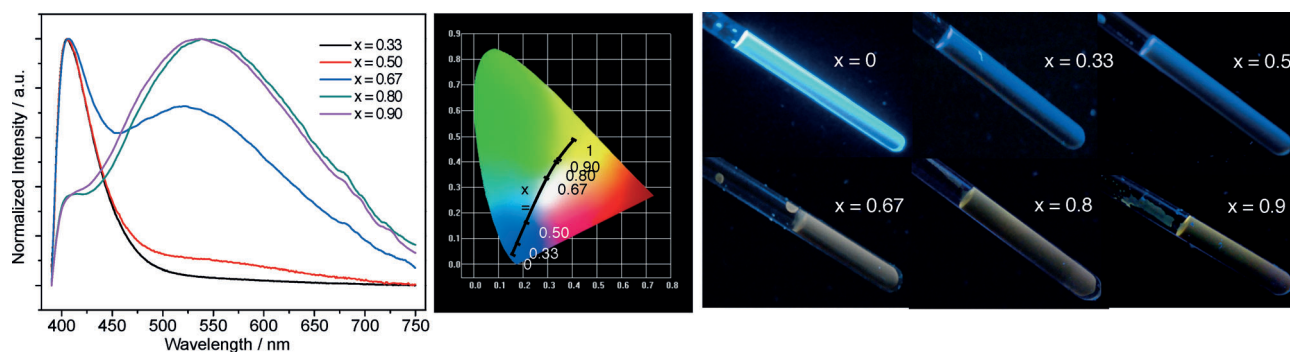
Figure 6. Normalized emission spectra of mixtures of the ILs [Chol][Sal] and [C$_4$C$_1$Py][Sal] excited at 340 nm (left). x is the molar fraction of [C$_4$C$_1$Py][Sal], that is, $x = (n[C_4C_1Py][Sal])/(n[Chol][Sal] + n[C_4C_1Py][Sal])$. Calculated color coordinates in the CIE color space of each mixture excited at 340 nm (center). $x = 0$ corresponds to pure [Chol][Sal], whereas $x = 1$ corresponds to pure [C$_4$C$_1$Py][Sal] excited at 410 nm. Photos of the IL mixtures in quartz tubes under 366 nm UV excitation (right).

closest to pure white light is when $x = 0.67$, that is, at a ratio [C$_4$C$_1$Py]/[Chol] of 2:1.

Conclusion

A range of ionic liquids based on the salicylate anion have been synthesized and their thermal, structural, and photophysical properties investigated. Firstly DSC confirmed all compounds were synthesized as ionic liquids, with melting transitions lower than 100 °C. Salicylate coupled with 1,3-dodecylmethylimidazolium gave an IL exhibiting a supercooled ionic liquid-crystal phase, identified as SmC by using POM and SAXS. 2D ^{1}H-^{1}H ROESY NMR spectroscopy identified strong ion-pair interactions in the case of pyridinium-based cations. Photoluminescence studies of these different compounds showed that the corresponding cation has a great influence on the emission intensity and color, which could be related back to structural aspects and interionic interactions. As a result, these compounds represent high intensity soft luminescent materials, presenting high quantum yields, and whose facile modification could result in emission of a desired color.

Experimental Section

Materials

Redistilled 1-methylimidazole ($>99\%$, Sigma Aldrich), 4-methylpyridine (98%, ABCR), quinoline (97%, ABCR), bromoethane (98%, ABCR), 1-chlorobutane (98%, ABCR), 1-chlorododecane, (97%, ABCR), choline chloride (99%, Acros Organics), trihexyltetradecylphosphonium chloride ($>95\%$, Io-li-tec), and sodium salicylate (99%, ABCR) were used as received.

Methods

NMR spectroscopy: ^{1}H, solution NMR data were collected at room temperature on a Bruker AC 200 MHz spectrometer, and spectra calibrated with respect to the residual solvent peak of [D$_6$]DMSO. 2D ^{1}H ROESY NMR experiments were carried out on a Bruker AC 250 MHz spectrometer.

Elemental analysis: Elemental analyses were performed using a Vario EL CHNOS analyzer (Elementar Analysensysteme GmbH,

Hanau, Germany). Helium was used as the flux gas and the samples combusted at 1150 °C using a WO$_3$ catalyst for conversion to NO$_x$, H$_2$O, CO$_2$ and SO$_2$. NO$_x$ is reduced to N$_2$ over Cu at 850 °C. Resultant gases were detected individually by using thermal conductivity.

Karl Fischer titration: The titration was performed by using a 831 KF Karl Fischer Coulometer (Metrohm Ion Analysis, Herisau, Switzerland). Water is titrated using iodine, generated directly in the electrolyte by electrochemical means. The end point is found voltametrically by applying an alternating current of constant strength to a double Pt electrode. Liquid samples were injected directly into the device, whereas for solid and viscous samples, the water content of known dichloromethane solutions were determined. The water content of the dichloromethane was also found and the water content of the sample could be calculated.

Ion chromatography: Ion exchange chromatography (IC) was conducted by using two Metrohm 882 IC Compact Systems, one for cations and one for anions using Metrohm IC Professional MF conductivity detectors. Data were processed by using Metrohm MagIC Net 2.4 Professional. A calibration for the quantitative analysis was carried out by using a seven point calibration curve (0.5–10 ppm) with FLUKA multi-ion standards and validated with a 10 ppm standard before measurements. The cation system is equipped with a Metrohm Metrosep C4 pre-column and a Metrohm Metrosep C4 150×4 cation main column. HNO$_3$ (1.7 mmol L^{-1}) and dipiccolinic acid (0.7 mmol L^{-1}) in a mixture of acetonitrile (20 vol.%) and pure water (80 vol.%) were used as the eluent for the cation column. The anion system is equipped with a Metrohm Metrosep A Supp 4/5 pre-column, a Metrohm Metrosep A Supp 4 150×5 anion main column and a Metrosep A trap column. Additionally, the anion is equipped with a chemical suppressor (Metrohm MSM, regenerated periodically with 100 mmol L^{-1} H$_2$SO$_4$) and a carbon dioxide suppressor (Metrohm MCS) for further signal improvement. As eluent for the anion column, sodium carbonate (3.2 mmol L^{-1}) and sodium bicarbonate (1 mmol L^{-1}) were used in a mixture of acetonitrile (20 vol.%) and pure water (80 vol.%).

Ionic liquid syntheses: For imidazolium and pyridinium ionic liquids, standard quaternization reactions were undertaken to obtain the necessary bromide (for [C$_2$C$_1$Im], [C$_2$C$_1$Py], and [C$_4$C$_1$Py]) or chloride (for [C$_4$C$_1$Im] and [C$_{12}$C$_1$Im] salts).[17] In each case, the anion metathesis was undertaken according to the following procedure resulting in quantitative yields.

Choline salicylate: Choline chloride (5.0 g, 35.8 mmol) and sodium salicylate (5.7 g, 35.8 mol) were stirred together in dry acetone

(50 mL) for 72 h. The white precipitate that formed was filtered off and the solvent removed in vacuo. Cold dry dichloromethane (100 mL) was added to the resultant liquid, and the resulting precipitate filtered off over Celite. The solvent was removed and the resulting liquid was dried in vacuo at 50 °C for a period of at least 72 h. The product was obtained as a yellow-tinted clear liquid in quantitative yield. ^{1}H NMR (200 MHz, [D$_6$]DMSO): $\delta = 15.95$ (s, 1 H, phenolic-O*H*), 7.74 (d, 1 H, CH-C*H*=C-COO$^-$), 7.16 (t, 1 H, C*H*-CH=C-COO$^-$), 6.67 (d, 1 H, CH-C*H*=C-OH), 6.64 (t, 1 H, C*H*-CH=C-OH), 6.13 (s, 1 H, CH$_2$O*H*), 3.89 (t, 1 H, N-C*H*$_2$), 3.47 (t, 1 H, C*H*$_2$OH), 3.16 ppm (s, 9 H, N(C*H*$_3$)$_3$); elemental analysis calcd (%) for C$_{12}$H$_{19}$NO$_4$: N 5.81; C 59.73; H 7.94; found: N 5.64; C 56.34; H 8.09. Water content (Karl Fischer): 222 ppm. Ion chromatography: Na$^+$: 0.60 wt.%; Cl$^-$: 0.28 wt.%.

Trihexyl(tetradecyl)phosphonium salicylate: ^{1}H NMR (200 MHz, [D$_6$]DMSO): $\delta = 16.52$ (s, 1 H, *H*), 7.67 (d, 1 H, CH-C*H*=C-COO$^-$), 6.59 (t, 1 H, C*H*-CH=C-COO$^-$), 6.55 (d, 1 H, CH-C*H*=C-OH), 2.21 (m, 8 H, N-C*H*$_2$), 1.24 (m, 48 H, C*H*$_2$CH$_2$CH$_2$), 0.87 ppm (m, 12 H, C*H*$_3$); elemental analysis calcd (%) for C$_{39}$H$_{73}$O$_3$P: C 75.43; H 11.85; found: C 70.28; H 11.01. Water content (Karl Fischer): 136 ppm. Ion chromatography: Na$^+$: 0.14 wt.%; Cl$^-$: 0.67 wt.%.

1-Ethyl-3-methylimidazolium salicylate: ^{1}H NMR (200 MHz, [D$_6$]DMSO): $\delta = 16.$ 11(s, 1 H, O*H*), 9.43 (s, 1 H, N-C*H*-N), 7.85 (s, 1 H, N-C*H*-CH-N), 7.76 (s, 1 H, N-CH-C*H*-N), 7.69 (d, 1 H, CH-C*H*=C-COO$^-$), 7.12 (t, 1 H, C*H*-CH=C-COO$^-$), 6.61 (d, 1 H, CH-C*H*=C-OH), 6.59 (t, 1 H, C*H*-CH=C-OH), 4.21 (q, 2 H, N-C*H*$_2$-CH$_3$), 3.87 (s, 3 H, N-C*H*$_3$), 1.39 ppm (t, 3 H, N-CH$_2$-C*H*$_3$); elemental analysis calcd (%) for C$_{13}$H$_{16}$N$_2$O$_3$: N 11.28; C 62.89; H 6.50; found: N 9.92; C 61.81; H 6.15. Water content (Karl Fischer): 462 ppm. Ion chromatography: Na$^+$: 0.16 wt.%; Br$^-$: 1.3 wt.%.

1-Butyl-3-methylimidazolium salicylate: ^{1}H NMR (200 MHz, [D$_6$]DMSO): $\delta = 16.$ 11(s, 1 H, O*H*), 9.43 (s, 1 H, N-C*H*-N), 7.80 (s, 1 H, N-C*H*-CH-N), 7.72 (d, 1 H, CH-C*H*=C-COO$^-$), 7.72 (s, 1 H, N-CH-C*H*-N), 7.14 (t, 1 H, C*H*-CH=C-COO$^-$), 6.64 (d, 1 H, CH-C*H*=C-OH), 6.61 (t, 1 H, C*H*-CH=C-OH), 4.16 (t, 2 H, N-C*H*$_2$-CH$_2$-), 3.87 (s, 3 H, N-C*H*$_3$), 1.73 (qn, 2 H, N-CH$_2$-C*H*$_2$-), 1.21 (sx, 2 H, CH$_2$-C*H*$_2$-CH$_3$), 0.84 ppm (t, 3 H, CH$_2$-C*H*$_3$); elemental analysis calcd (%) for C$_{15}$H$_{20}$N$_2$O$_3$: N 10.81; C 65.20; H 7.30; found: N 10.17; C 62.25; H 8.03. Water content (Karl Fischer): 236 ppm. Ion chromatography: Na$^+$: 0.096 wt.%; Cl$^-$ 0.67 wt.%.

1-Dodecyl-3-methylimidazolium salicylate: ^{1}H NMR (200 MHz [D$_6$]DMSO): $\delta = 16.11$ (s, 1 H, O*H*), 9.17 (s, 1 H, N-C*H*-N), 7.77 (s, 1 H, N-C*H*-CH-N), 7.70 (s, 1 H, N-CH-C*H*-N), 7.64 (d, 1 H, CH-C*H*=C-COO$^-$), 7.09 (t, 1 H, C*H*-CH=C-COO$^-$), 6.57 (d, 1 H, CH-C*H*=C-OH), 6.55 (t, 1 H, C*H*-CH=C-OH), 4.14 (q, 2 H, N-C*H*$_2$-CH$_3$), 3.85 (s, 3 H, N-C*H*$_3$), 1.76 (2 H, N-CH$_2$-C*H*$_2$-), 1.24 (m, 18 H, -(C*H*$_2$)$_9$-CH$_3$), 0.85 ppm (t, 3 H, -CH$_2$-C*H*$_3$); elemental analysis calcd (%) for C$_{23}$H$_{36}$N$_2$O$_3$: N 7.21; C 71.10; H 9.34; found: N 6.64; C 66.74; H 9.57. Water content (Karl Fischer): 181 ppm. Ion chromatography: Na$^+$: 0.44 wt.%; Cl$^-$: 0.36 wt.%.

1-Ethyl-4-methylpyridinium salicylate: ^{1}H NMR (200 MHz, [D$_6$]DMSO): $\delta = 16.24$ (s, 1 H, O*H*), 8.99 (d, 2 H, C*H*=N-CH (pyridinium)), 7.97 (d, 2 H, CH=C-C*H* (pyridinium)), 7.67 (d, 1 H, CH-C*H*=C-COO$^-$), 7.12 (t, 1 H, C*H*-CH=C-COO$^-$), 6.60 (d, 1 H, CH-C*H*=C-OH), 6.58 (t, 1 H, C*H*-CH=C-OH), 4.58 (q, 2 H, N-C*H*$_2$CH$_3$), 2.58 (s, 3 H, C-C*H*$_3$), 1.50 ppm (t, 3 H, CH$_2$CH$_2$C*H*$_3$); elemental analysis calcd (%) for C$_{15}$H$_{17}$NO$_3$: N 5.40; C 69.48; H 6.61; found: N 5.16; C 66.34; H 5.86. Water content (Karl Fischer): 589 ppm. Ion chromatography: Na$^+$: 0.062 wt.%; Br$^-$: 0.080 wt.%.

1-Butyl-4-methylpyridinium salicylate: ^{1}H NMR (200 MHz, [D$_6$]DMSO): $\delta = 16.24$ (s, 1 H, O*H*), 8.99 (d, 2 H, C*H*=N-C*H* (pyridinium)), 7.97 (d, 2 H, CH=C-C*H* (pyridinium)), 7.67 (d, 1 H, CH-C*H*=C-COO$^-$), 7.12 (t, 1 H, C*H*-CH=C-COO$^-$), 6.60 (d, 1 H, CH-C*H*=C-OH), 6.58 (t, 1 H, C*H*-

CH=C-OH), 4.55 (t, 2 H, N-C*H*$_2$CH$_2$), 2.59 (s, 3 H, C-C*H*$_3$), 1.86 (qn, 2 H, -CH$_2$C*H*$_2$CH$_2$-), 1.26 (sx, 2 H, CH$_2$C*H*$_2$CH$_3$), 0.88 ppm (t, 3 H, CH$_2$CH$_2$C*H*$_3$); elemental analysis calcd (%) for C$_{17}$H$_{21}$NO$_3$: N 4.87; C 71.1; H 7.37; found: N 4.23; C 66.89; H 6.74. Water content (Karl Fischer): 566 ppm. Ion chromatography: Na$^+$: 0.067 wt.%; Br$^-$: 0.27 wt.%.

Differential scanning calorimetry: DSC measurements were performed on a computer-controlled Phoenix DSC 204 F1 thermal analyzer (Netzsch, Selb, D) under a constant flow of argon gas. Samples of ≈ 5 mg were cold-sealed in aluminium crucibles. Experimental data are displayed in such a way that exothermic peaks occur at negative heat flow and endothermic peaks at positive heat flow. DSC runs included heating and subsequent cooling at 10 °C min^{-1}. Transition temperatures are defined as the onset of the respective thermal processes.

Polarizing optical microscopy: POM images were acquired by using an Axio Imager A1 microscope (Carl Zeiss MicroImaging GmbH, Göttingen, Germany) equipped with a hot stage, THMS600 (Linkam Scientific Instruments Ltd, Surrey, UK), and a Linkam TMS 94 (Linkam Scientific Instruments Ltd, Surrey, UK) temperature controller and crossed polarizers. Images were recorded at a magnification of 100× as video with a digital camera after initial heating during the cooling stage. Heating and cooling rates were 5 K min^{-1}$^{-1}$. For measurement, the samples were placed under argon between two cover slips, which were sealed with two-component adhesive (UHU plus 300, UHU GmbH & Co. KG, Bühl, Germany).

Temperature-dependent small-angle X-ray scattering: SAXS measurements were carried out at the A2 Beamline of DORIS III, Hasylab, DESY, Hamburg, Germany, at a fixed wavelength of 1.5 Å. The data were collected with a MarCCD detector. The detector was calibrated with silver behenate. The sample-detector position was fixed at 635.5 mm. For measurements, the samples were placed in a copper sample holder between aluminium foil. The sample temperature was controlled by a JUMO IMAGO 500 multi-channel process and program controller. Data reduction and analysis, correction or background scattering and transmission were carried out by using a2tool (Hasylab).

Powder X-ray diffraction: The powder X-ray diffraction measurements were carried out on a G670 diffractometer with an image plate detector (Huber, Rimsting, D) operating with Mo$_{K\alpha}$ radiation.

UV/Vis absorption spectroscopy: Visible absorption spectra were measured at room temperature on a Cary 50 spectrometer (Varian, Palo Alto, USA). Molar ethanolic solutions (1.0×10^{-5}) were loaded into quartz cuvettes (optical special-purpose (OS) glass).

Photoluminescence measurements: Fluorescence and phosphorescence measurements were performed on a Fluorolog FL 3–22 spectrometer (Horiba Jobin Yvon, Unterhachingen, D). A choice between a continuous xenon lamp with 450 W for fluorescence and a pulsed xenon lamp for phosphorescence measurements is possible. Double gratings for the excitation and emission spectrometer are applied as monochromators. The signal is detected with a photomultiplier. For measurement, powdered samples were filled into silica tubes and carefully positioned in the incoming beam in the sample chamber. Quantum yield measurements were achieved with aid of an integrating sphere. For solid samples, optical standard BaSO$_4$ was used as a reflectance standard, whereas for liquid samples, distilled water was used. Measurements were carried out at least three times and deviations were used to calculate the error.

[1] B. Geffroy, P. L. Roy, C. Prat, *Polym. Int.* **2006**, *55*, 572.

[2] L. S. Hung, C. H. Chen, *Mater. Sci. Eng. R* **2002**, *39*, 143.

[3] Y. Chen, D. Ma, *J. Mater. Chem.* **2012**, *22*, 18718.

[4] N. T. Kalyani, S. J. Dhoble, *Renewable Sustainable Energy Rev.* **2012**, *16*, 2696.

[5] Y. Ohmori in *Organic Electronics* (Ed.: F. So), CRC, Boca Raton, **2012**, p. 511.

[6] F. So, J. Kido, P. Burrows, *MRS Bull.* **2008**, *33*, 663.

[7] L. Shi, Z. Liu, G. Dong, L. Duan, Y. Qiu, J. Jia, W. Guo, D. Zhao, D. Cui, X. Tao, *Chem. Eur. J.* **2012**, *18*, 8092.

[8] C. Poriel, J. Rault-Berthelot, D. Thirion, F. Barrière, L. Vignau, *Chem. Eur. J.* **2011**, *17*, 14031.

[9] F. J. Duarte, *Opt. Photonics News* **2003**, *14*, 20.

[10] K. Binnemans, *Chem. Rev.* **2009**, *109*, 4283.

[11] T. Terai, H. Ito, K. Kikuchi, T. Nagano, *Chem. Eur. J.* **2012**, *18*, 7377.

[12] E. B. van der Tol, H. J. van Ramesdonk, J. W. Verhoeven, F. J. Steemers, E. G. Kerver, W. Verboom, D. N. Reinhoudt, *Chem. Eur. J.* **1998**, *4*, 2315.

[13] F. So, D. Kondakov, *Adv. Mater.* **2010**, *22*, 3762.

[14] T. Woike, A. Schuy, J. Krause, D. Schaniel, S. Pitula, A.-V. Mudring, DE 102009000784A1 20100812, Germany, **2010**.

[15] S. Pitula, PhD Thesis, *Luminescent Ionic Liquids*, Universität zu Köln (Cologne), **2010**.

[16] J. P. Hallett, T. Welton, *Chem. Rev.* **2011**, *111*, 3508.

[17] P. Wasserscheid, T. Welton, *Ionic Liquids in Synthesis*, Wiley-VCH, Weinheim, **2007**.

[18] T. Welton, *Chem. Rev.* **1999**, *99*, 2071.

[19] T. Welton, *Fundamentals of Catalysis in Nonaqueous Ionic Liquids, Vol. 2*, Wiley-VCH, Weinheim, **2005**.

[20] A. K. Chakraborti, S. R. Roy, *J. Am. Chem. Soc.* **2009**, *131*, 6902.

[21] H. P. Steinrück, J. Libuda, P. Wasserscheid, T. Cremer, C. Kolbeck, M. Laurin, F. Maier, M. Sobota, P. S. Schulz, M. Stark, *Adv. Mater.* **2011**, *23*, 2571.

[22] P. S. Campbell, A. Podgorsek, T. Gutel, C. C. Santini, A. A. H. Padua, M. F. Costa Gomes, F. Bayard, B. Fenet, Y. Chauvin, *J. Phys. Chem. B* **2010**, *114*, 8156.

[23] A. Podgorsek, G. Salas, P. S. Campbell, C. C. Santini, A. A. H. Padua, M. F. Costa Gomes, B. Fenet, Y. Chauvin, *J. Phys. Chem. B* **2011**, *115*, 12150.

[24] C. P. Mehnert, *Chem. Eur. J.* **2005**, *11*, 50.

[25] X. Han, D. W. Armstrong, *Acc. Chem. Res.* **2007**, *40*, 1079.

[26] C. F. Poole, S. K. Poole, *J. Sep. Sci.* **2011**, *34*, 888.

[27] P. S. Campbell, C. C. Santini, Y. Chauvin, *Chim. Oggi* **2010**, *28*, 36.

[28] M. Armand, F. Endres, D. R. MacFarlane, H. Ohno, B. Scrosati, *Nat. Mater.* **2009**, *8*, 621.

[29] F. Endres, *Chem. Ing. Tech.* **2011**, *83*, 1485.

[30] J. Dupont, J. D. Scholten, *Chem. Soc. Rev.* **2010**, *39*, 1780.

[31] J. D. Scholten, B. C. Leal, J. Dupont, *ACS Catal.* **2012**, *2*, 184.

[32] J. D. Scholten, M. H. G. Prechtl, J. Dupont in *Handbook of Green Chemistry, Vol. 8* (Ed.: P. T. Anastas), Wiley-VCH, Weinheim, **2012**, p. 1.

[33] P. S. Campbell, C. C. Santini, F. Bayard, Y. Chauvin, V. Colliere, A. Podgorsek, M. F. Costa Gomes, J. Sa, *J. Catal.* **2010**, *275*, 99.

[34] P. S. Campbell, C. C. Santini, D. Bouchu, B. Fenet, K. Philippot, B. Chaudret, A. A. H. Padua, Y. Chauvin, *Phys. Chem. Chem. Phys.* **2010**, *12*, 4217.

[35] R. E. Morris, *Angew. Chem.* **2008**, *120*, 450; *Angew. Chem. Int. Ed.* **2008**, *47*, 442.

[36] P. S. Campbell, M. H. G. Prechtl, C. C. Santini, P.-H. Haumesser, *Curr. Org. Chem.* **2013**, *17*, 414.

[37] K. Richter, A. Birkner, A.-V. Mudring, *Phys. Chem. Chem. Phys.* **2011**, *13*, 7136.

[38] K. Richter, A. Birkner, A.-V. Mudring, *Angew. Chem.* **2010**, *122*, 2481; *Angew. Chem. Int. Ed.* **2010**, *49*, 2431.

[39] G. Wang, A.-V. Mudring, *Crystals* **2011**, *1*, 22.

[40] A. Kokorin, *Ionic Liquids: Applications and Perspectives*, InTech, Rijeka, **2011**.

[41] A. Getsis, A.-V. Mudring, *Eur. J. Inorg. Chem.* **2011**, 3207.

[42] S. Tang, A.-V. Mudring, *Cryst. Growth Des.* **2011**, *11*, 1437.

[43] A. Getsis, S. Tang, A.-V. Mudring, *Eur. J. Inorg. Chem.* **2010**, 2172.

[44] S. Pitula, A.-V. Mudring, *Chem. Eur. J.* **2010**, *16*, 3355.

[45] A. Tokarev, J. Larionova, Y. Guari, C. Guerin, J. M. Lopez-de-Luzuriaga, M. Monge, P. Dieudonne, C. Blanc, *Dalton Trans.* **2010**, *39*, 10574.

[46] K. Lunstroot, K. Driesen, P. Nockemann, L. Viau, P. H. Mutin, A. Vioux, K. Binnemans, *Phys. Chem. Chem. Phys.* **2010**, *12*, 1879.

[47] Q. Ju, P. S. Campbell, A.-V. Mudring, *J. Mater. Chem. B* **2013**, *1*, 179.

[48] J. Cybinska, C. Lorbeer, A.-V. Mudring, *J. Mater. Chem.* **2012**, *22*, 9505.

[49] C. Lorbeer, J. Cybinska, E. Zych, A. V. Mudring, *Opt. Mater.* **2011**, *34*, 336.

[50] P. Ghosh, S. Tang, A.-V. Mudring, *J. Mater. Chem.* **2011**, *21*, 8640.

[51] J. Cybinska, C. Lorbeer, E. Zych, A.-V. Mudring, *ChemSusChem* **2011**, *4*, 595.

[52] C. Lorbeer, J. Cybinska, A.-V. Mudring, *Cryst. Growth Des.* **2011**, *11*, 1040.

[53] N. von Prondzinski, J. Cybinska, A.-V. Mudring, *Chem. Commun.* **2010**, *46*, 4393.

[54] C. Lorbeer, J. Cybinska, A.-V. Mudring, *Chem. Commun.* **2010**, *46*, 571.

[55] P. S. Campbell, C. Lorbeer, J. Cybinska, A. V. Mudring, *Adv. Funct. Mater.* **2013**, *23*, 2924 – 2931.

[56] A. Getsis, A. V. Mudring, *Cryst. Res. Technol.* **2008**, *43*, 1187.

[57] A. Paul, P. K. Mandal, A. Samanta, *J. Phys. Chem. B* **2005**, *109*, 9148.

[58] I. Bandres, M. Haro, B. Giner, H. Artigas, C. Lafuente, *Phys. Chem. Liq.* **2011**, *49*, 192.

[59] Z. Chen, S. Zhang, X. Qi, S. Liu, Q. Zhang, Y. Deng, *J. Mater. Chem.* **2011**, *21*, 8979.

[60] Q. Zhang, B. Yang, S. Zhang, S. Liu, Y. Deng, *J. Mater. Chem.* **2011**, *21*, 16335.

[61] A. J. Boydston, C. S. Pecinovsky, S. T. Chao, C. W. Bielawski, *J. Am. Chem. Soc.* **2007**, *129*, 14550.

[62] A. J. Boydston, P. D. Vu, O. L. Dykhno, V. Chang, A. R. Wyatt, A. S. Stockett, E. T. Ritschdorff, J. B. Shear, C. W. Bielawski, *J. Am. Chem. Soc.* **2008**, *130*, 3143.

[63] J.-F. Huang, H. Luo, C. Liang, I. W. Sun, G. A. Baker, S. Dai, *J. Am. Chem. Soc.* **2005**, *127*, 12784.

[64] J. D. Holbrey, K. R. Seddon, *J. Chem. Soc. Dalton Trans.* **1999**, 2133.

[65] M. Yang, B. Mallick, A.-V. Mudring, *Cryst. Growth Des.*, **2013**, *13*, 3068 – 3077.

[66] B. Valeur, M. N. Berberan-Santos, *Molecular Fluorescence: Principles and Applications*, 2nd ed., Wiley-VCH, Weinheim, **2012**.

[67] A. Mishra, R. K. Behera, P. K. Behera, B. K. Mishra, G. B. Behera, *Chem. Rev.* **2000**, *100*, 1973.

[68] J. B. Birks, L. G. Christophorou, *Spectrochim. Acta* **1963**, *19*, 401.

[69] J. N. A. Canongia Lopes, A. A. H. Padua, *J. Phys. Chem. B* **2006**, *110*, 3330.

[70] Y. Wang, G. A. Voth, *J. Am. Chem. Soc.* **2005**, *127*, 12192.

[71] A. Triolo, O. Russina, H.-J. Bleif, E. Di Cola, *J. Phys. Chem. B* **2007**, *111*, 4641.

[72] D. Frezzato, F. Rastrelli, A. Bagno, *J. Phys. Chem. B* **2006**, *110*, 5676.

[73] W. Marczak, S. P. Verevkin, A. Heintz, *J. Solution Chem.* **2003**, *32*, 519.

[74] J. Oshima, T. Yoshihara, S. Tobita, *Chem. Phys. Lett.* **2006**, *423*, 306.

[75] W. M. Yen, S. Shionoya, H. Yamamoto, *Phosphor Handbook*, 2nd ed., CRC, Boca Raton, **2006**.